Nanoscale

PAPER

Cite this: *Nanoscale*, 2018, **10**, 19557

Plasmonic isomers *via* DNA-based self-assembly of gold nanoparticles†

Laurent Lermusiaux* and Alison M. Funston *

Received 9th July 2018,
Accepted 1st October 2018

DOI: 10.1039/c8nr05509b

rsc.li/nanoscale

Developments in DNA nanotechnology offer control of the self-assembly of materials into discrete nanostructures. Within this paradigm, pre-assembled DNA origami with hundreds of DNA strands allows for precise and programmable spatial positioning of functionalised nanoparticles. We propose an alternative approach to construct multiple, structurally different, nanoparticle assemblies from just a few complementary nanoparticle-functionalised DNA strands. The approach exploits local minima in the potential energy landscape of hybridised nanoparticle-DNA structures by employing kinetic control of the assembly. Using a four-strand DNA template, we synthesise five different 3D gold nanoparticle (plasmonic) tetrameric isomers, akin to molecular structural isomers. The number of different structures formed using this approach for a set of DNA strands represents a combinatorial library, which we summarise in a hybridisation pathway tree and use to achieve deposition of tetrahedral assemblies onto substrates in high yield. The ability to program nanoparticle self-assembly pathways gives unprecedented access to unique plasmonic nanostructures.

Introduction

The specific recognition of the Watson–Crick base pairing as a mechanism to form three-dimensional networks of nucleic acids underpins what we now refer to as DNA nanotechnology.[1] The subsequent self-assembly of discrete DNA structures into desired shapes[2,3] *via* DNA origami[4–6] techniques has proven to be a key enabling technology in this area. The fundamental principle governing such DNA self-assemblies is the design of single-stranded DNA (ss-DNA) with sub-sequences that are complementary to one or more other DNA strands. Upon hybridisation of all complementary sequences, a thermodynamically stable nanostructure is generated. Consequently, DNA self-assembly generally requires an annealing step to promote the cooperative folding of the strands[7,8] and ensure high yields of the desired structure by favouring the lowest-energy product, irrespective of the chemical pathway used. As a result, there has been relatively little interest in studying these pathways, which, if better understood, could be optimised to increase assembly yields[9] or promote conformational dynamics.[10] In the absence of the annealing step, a myriad of kinetically controlled structures are produced across a potential energy landscape, with each structure corresponding to a local minimum of the energy profile.[9,11] The number of different structures produced theoretically reflects a vast combinatorial library, which contains all the possible combinations of assembling the different ss-DNA.

The overarching advantage of DNA-based techniques in nanoscience is the ability to use the DNA scaffold as a means for directing the position of other species which interact with the DNA, including other biological moieties, fluorophores and nanoparticles.[12,13] Specifically, thiol-modified DNA can be used to assemble gold nanoparticles into discrete structures[14,15] for applications such as colorimetric biosensors,[16–18] biological probes,[19] plasmonic antennas[20] and plasmon rulers.[21,22] Recently, pre-assembled DNA origami used as scaffolds enabled the fabrication of large gold nanoparticle superstructures,[23–28] requiring numerous DNA strands to design a single shape. To overcome the scalability and cost limitations of such DNA-based assemblies, alternative approaches based on the multiple functionalisation of individual nanoparticles have been developed to minimise the number of DNA strands.[29–31] All these approaches commonly aim to produce thermodynamically stable products by engineering the DNA attached to the particles with a single recognition site, which implies a limited number of possible nano-assembly structures per DNA set. Moreover, the geometry of self-assembled nanostructures in solution depends on a

ARC Centre of Excellence in Exciton Science and School of Chemistry, Monash University, Clayton, VIC, 3800, Australia. E-mail: laurent.lermusiaux@monash.edu, alison.funston@monash.edu

†Electronic supplementary information (ESI) available: DNA sequences; summary of the different experimental conditions; hybridisation pathway tree of the asymmetrical assembly; complementary electrophoresis gels and additional cross-sections; TEM-based tetramer yield estimation; additional conventional and cryogenic electron microscopy images; diameter distribution of gold nanoparticles; statistical analysis of cryo-EM images; extinction spectra. See DOI: 10.1039/c8nr05509b

complex combination of attractive and repulsive forces, which are dependent on the ionic strength,[22,32] temperature[33] and nanocrystal surface chemistry.[34,35] These parameters can frustrate the shape of a pre-designed DNA scaffold, potentially limiting the utility of fully hybridised templates.

We demonstrate here the possibility of harvesting the various kinetically controlled products of DNA self-assemblies using nanoparticle-functionalised DNA strands by exploiting the potential energy landscape of the DNA-nanoparticle hybrids. This approach leads to the potentially facile production of a number of discrete three-dimensional isomeric assemblies of nanoparticles from a given set of ss-DNA, akin to molecular structural isomers.[36–38] The structures synthesised are at the local minima of the DNA-nanoparticle system and are therefore influenced by the electrostatic repulsions and steric hindrance of the charged nanoparticles[39] leading to preferentially produced structures. We provide a simple set of rules for the formation of specific structures *via* a structure library and chemical pathway tree. In this context, the four-strand tetrahedral DNA template, which is the simplest DNA three-dimensional origami, is used to demonstrate the reproducible synthesis of various gold nanoparticle tetrameric isomers, using various chemical pathways. This DNA set, which only requires a thermal treatment to produce a high yield of single diastereoisomers,[40] is of great importance in the field of DNA nanotechnology, being a promising tool for drug delivery thanks to its high cellular uptake.[41] The power of the approach is demonstrated by its exploitation to facilitate deposition of tetramers into three-dimensional tetrahedra with high yield.[42,43]

Results and discussion

Gold nanoparticle tetramer synthesis with a tetrahedral DNA template

Fig. 1c shows a TEM image of one of the tetramers formed by the self-assembly of a gold nanoparticle-functionalised DNA template. The four-strand DNA sets employed are designed to form a tetrahedral scaffold made of six 30-base long double-stranded DNA (ds-DNA) edges separated by three thymine nucleobase hinges to facilitate the bending of the DNA at the corners (ESI Fig. S1†).[40,44] To form the tetramer, a 10 nm gold nanoparticle is conjugated to the thiolated 5′-end of each of the four ss-DNA (structures 1 to 8 in Fig. 1a) and each nanoparticle is functionalised with only one ss-DNA. Assembly of the gold nanoparticle-functionalised DNA template is carried out *via* either a single-step method where all four ss-DNA are hybridised together (pathways P4 and P8 in Fig. 1a), or a two-step process whereby two pairs of dimers are produced and purified, and subsequently hybridised together. This latter assembly also poses the possibility of the initially formed dimers being hybridised with DNA sub-sequences located either symmetrically (P1 to P3) or asymmetrically (P5 to P7) with respect to the gold nanoparticles. Purification of the structures is carried out at each of the individual steps *via* electrophoresis (ESI Fig. S3†).

The gel in Fig. 1b shows separate bands for each of the assembly products of a dimer (left column) and of the tetramers formed *via* each pathway. The electrophoretic purification of dimers shows almost no larger structures confirming that each nanoparticle is attached to a single DNA strand (additional gels shown in ESI Fig. S3†). Significant variation in electrophoretic mobility among the tetramer bands for each assembly pathway is apparent on the normalised cross-sections shown in Fig. 1d and e for pathways P1 to P4 and P8 (see ESI Fig. S4† for the other pathways). This establishes that the tetramers produced have different hydrodynamic volumes, confirming that they are structurally different (*i.e.* tetrameric isomers) and that the assembly pathways do not produce an identical product. The contents of the tetramer bands were confirmed to be tetramers by electron microscopy following their extraction from the gel (Fig. 1c and ESI Fig. S8†), with yields ranging from 45 to 85% (ESI Table S2†). The relative band positions for each assembly pathway were reproducible (see ESI Fig. S6†).

The formation of different tetrameric isomers occurs due to different degrees of hybridisation of the DNA scaffold in each of the structures. For each DNA set, there are 42 assembly combinations of DNA strands that can produce tetramers, with either three, four, five or six hybridised sub-sequences (Table 1). Because of symmetries in the DNA sets, these 42 tetramers can be classified into 18 (resp. 26) different structural isomers for the symmetrical (resp. asymmetrical) DNA set (Fig. 2d and ESI Fig. S2†). The presence of partially hybridised tetramers also accounts for the significant number of structures with more than four spheres produced by each pathway, resulting from inter-structure hybridisation. Fig. 1d distinctly displays two peaks with lower electrophoretic mobility than the tetramer which likely correspond to discrete assemblies of six and eight particles. To differentiate each isomer, we use a naming system that reports all the positions of the double-stranded sub-sequences on their respective DNA strand (Fig. 2d).

It is clear that the DNA self-assembly presented here is a step-wise hybridisation process starting from three ds-DNA tetramers. In the two-step assembly, dimers with smaller inter-particle distances lead to the production of tetramers of smaller volumes (Fig. 1f), indicating that the sub-sequences hybridised within the dimers most likely remain hybridised in the tetramer, whereas the single-step assembly can theoretically yield all isomers. Consequently, we can easily determine all the possible isomers that can be produced by each pathway using their names, *e.g.* isomers assembled using pathway P2 must include the combination 2-2.

Hybridisation pathway tree

Although each pathway can potentially produce many isomers of different hydrodynamic volumes, the occurrence of distinct thin tetramer bands in the electrophoretic gel indicates that some isomers are preferentially synthesised in each pathway.

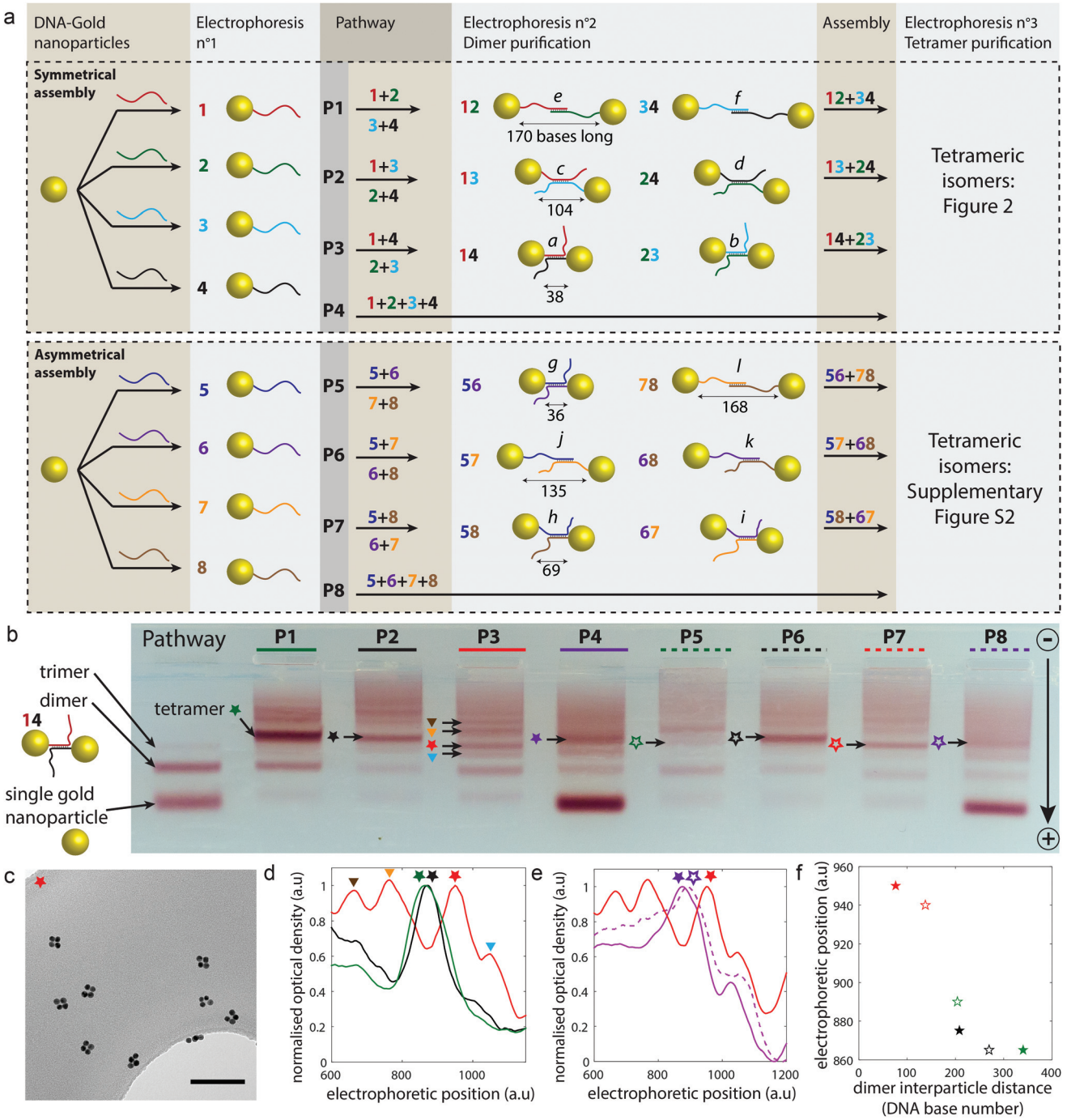

Fig. 1 Pathway-dependant synthesis of gold nanoparticle tetrameric isomers. (a) Schematic representation of different pathways (P1 to P8) to assemble gold nanoparticles into tetramers using two tetrahedral DNA scaffolds – symmetric (P1–P4) and asymmetric (P5–P8). (b) Electrophoretic purification of dimers assembled using a single DNA strand (example of structure 14 shown in left column) and of tetramers synthesised through eight different pathways. Tetramer bands are indicated by arrows and stars. Triangles indicate the electrophoretic band of trimers (cyan), 6-mer (orange) and 8-mer (brown) in pathway P3. (c) TEM image of tetramers obtained from pathway P3. Scale bar is 100 nm. (d,e) Cross-sections along the migration axis of the electrophoretic gel normalised and centred around the tetramer band for (d) pathways P1 (green line), P2 (black line) and P3 (red line), and for (e) pathways P3 (red line), P4 (purple dotted line) and P8 (purple solid line). (f) Electrophoretic position of the tetramer bands plotted against the total interparticle distance in dimers for pathways P1 to P3 and P5 to P7.

Therefore, the presence of charged nanoparticles sufficiently modifies the energy barriers of the different possible DNA hybridisation to consistently lead to specific isomers. Illustrative energy profile diagrams for the nanoparticle-functionalised DNA hybridisations are presented in Fig. 2a–c to qualitatively describe the effect of the presence of the nano-

Table 1 Summary of the 42 DNA hybridisation combinations that can produce a tetramer and the corresponding isomer structures of the symmetrical assembly scheme

Isomer	DNA hybridisation combination	Isomer	DNA hybridisation combination
1-1-2	a-b-c/a-b-d	1-1-2-3	a-b-c-e/a-b-c-f/a-b-d-e/a-b-d-f
1-1-3	a-b-e/a-b-f	1-1-3-3	a-b-e-f
1-2-3a	a-c-e/b-c-f/a-d-f/b-d-e	1-2-2-3	a-c-d-e/b-c-d-e/a-c-d-f/b-c-d-f
1-2-3b	a-c-f/a-d-e/b-c-e/b-d-f	1-2-3-3	a-c-e-f/a-d-e-f/b-c-e-f/b-d-e-f
1-3-3	a-e-f/b-e-f	2-2-3-3	c-d-e-f
2-3-3	c-e-f/d-e-f	1-1-2-2-3	a-b-c-d-e/a-b-c-d-f
1-2-2	a-c-d/b-c-d	1-1-2-3-3	a-b-c-e-f/a-b-d-e-f
2-2-3	c-d-e/c-d-f	1-2-2-3-3	a-c-d-e-f/b-c-d-e-f
1-1-2-2	a-b-c-d	1-1-2-2-3-3	a-b-c-d-e-f

Letters represent specific ds-DNA sub-sequences as shown in Fig. 1a. Isomer structures and names are detailed in Fig. 2d.

particles on the DNA hybridisation energetics. Here, the 30-base hybridisation events are represented by a single energy barrier,[45] with the energetics adapted according to the following. The energy level of the structures reflects the balance of competing effects: this decreases with an increasing number of ds-DNA, and increases with decreasing interparticle distances due to higher repulsions between the negatively charged spheres at small distances.[46] Also, the steric hindrance introduced by the nanoparticles, as well as their distance-dependant repulsions, favour the hybridisation of DNA sub-sequences located further away from the nanoparticles. Therefore, the energy barrier decreases when the distance between the DNA sub-sequences and the nanoparticle increases. This remark is validated by observing that the tetramers of the single-step assembly possess longer interparticle distances (Fig. 1e). There is therefore a correlation between the energy barrier and the energy of the formed structure, favouring the synthesis of stable products.

Using these considerations, we are able to identify the predominant tetrameric isomers in each pathway.

(1) For pathways P1 and P3, the competition initially occurs between neighbouring sub-sequences, presumably leading to the formation of both 3 ds-DNA structures with an excess of the larger one (Fig. 2a). However, for pathway P2, the competition takes place between the sub-sequences 1 and 3 and should exclusively lead to 2-2-3 (Fig. 2b). This reasoning can be extended to any further intra-tetramer hybridisation, *i.e.* hybridisations involving sub-sequences located further away from the charged nanoparticles are more likely to occur, yielding larger isomers (Fig. 2c).

(2) Hybridisation of two DNA strands into a helix requires some degree of freedom of the ss-DNA. Therefore, DNA hybridisation processes are not equivalent depending on whether they involve DNA strands with (dotted line DNA in Fig. 2d) or without (solid line DNA) free ends. If a given structure has either complementary sub-sequence with an end free, then it constitutes a reaction intermediate that will highly likely further react in the self-assembly process. In contrast, if the complementary sub-sequences of DNA have no free ends, their hybridisation requires the unlikely rotation of two nanoparticles around the forming helix axis. Moreover, because of topological constraints,[47] it is nearly impossible for isomers 1-1-3-3 and 1-1-2-3-3 to further hybridise since their remaining single-stranded sub-sequences are in position 2 with the surrounding sub-sequences 1 and 3 already hybridised.

Therefore, the complete pathway tree predicts that five isomers of the 18 possible are more likely to be produced by the two-step assembly. Those given by pathways P2 and P3 are 4 and 5 ds-DNA tetramers that result from intra-hybridisation of 3 or 4 ds-DNA intermediary structures with one DNA free end, that could also form larger assemblies by inter-structure hybridisation. Consequently, the yield of isomers favoured in pathways P2 and P3 is expected to be lower than the yield of the two favoured 3 ds-DNA isomers in pathway P1, which was experimentally confirmed (Fig. 1b).

Thermodynamics of the gold nanoparticle self-assembly

Optimisation of the electrophoretic gel allows the separation of the five isomers (see Fig. 3a for pathways P1 to P3). Two separate tetramer bands are observed for pathways P1 and P3 and a single band for pathway P2. The normalised cross-sections of the gel show that the relative hydrodynamic radii of isomers are 1-1-2-3-3 < 1-1-3-3 < 1-3-3 < 2-2-3-3 < 2-3-3 (Fig. 3b), as expected based on hybridisation in the DNA template. Specifically, the more ds-DNA sub-sequences and the closer they are positioned to the particles, the smaller the corresponding isomer. For pathways P1 and P3, larger isomers are produced in higher yield. These results are consistent with predictions of the hybridisation pathway for the number of isolable isomers, their relative amounts and sizes. Although our simple energy profiles were presented for illustrative purposes, the agreement between the predicted and obtained structures validates the model. The passivating ligand used, BSPP or PEG, did not affect the tetramer synthesis outcomes (Fig. 3a and c and ESI Fig. S5†).

The presence of charged nanoparticles modifies the energy landscape of the DNA self-assembly in a way that allows the kinetically controlled synthesis of specific isomers at room temperature. Decreasing electrostatic repulsions between gold nanoparticles with increased salt concentrations or using a thermal treatment to favour thermodynamically stable products could therefore lead to different products of the assembly. In order to modify tetramer products, additional salt to shield interparticle repulsion, and increased temperature to probe the thermodynamically favoured products, were utilised. A moderate thermal treatment (40 °C) and an increased NaCl concentration of 300 mM during assembly resulted in fewer yet identical isomers (Fig. 3d and e). Assembly carried out using a standard thermal treatment for the formation of the tetrahedral DNA scaffold,[40,41] *i.e.* mixing at 90 °C and cooling overnight, resulted in nearly no tetramers and a large excess of monomers and aggregates (Fig. 3f). The increased monomer

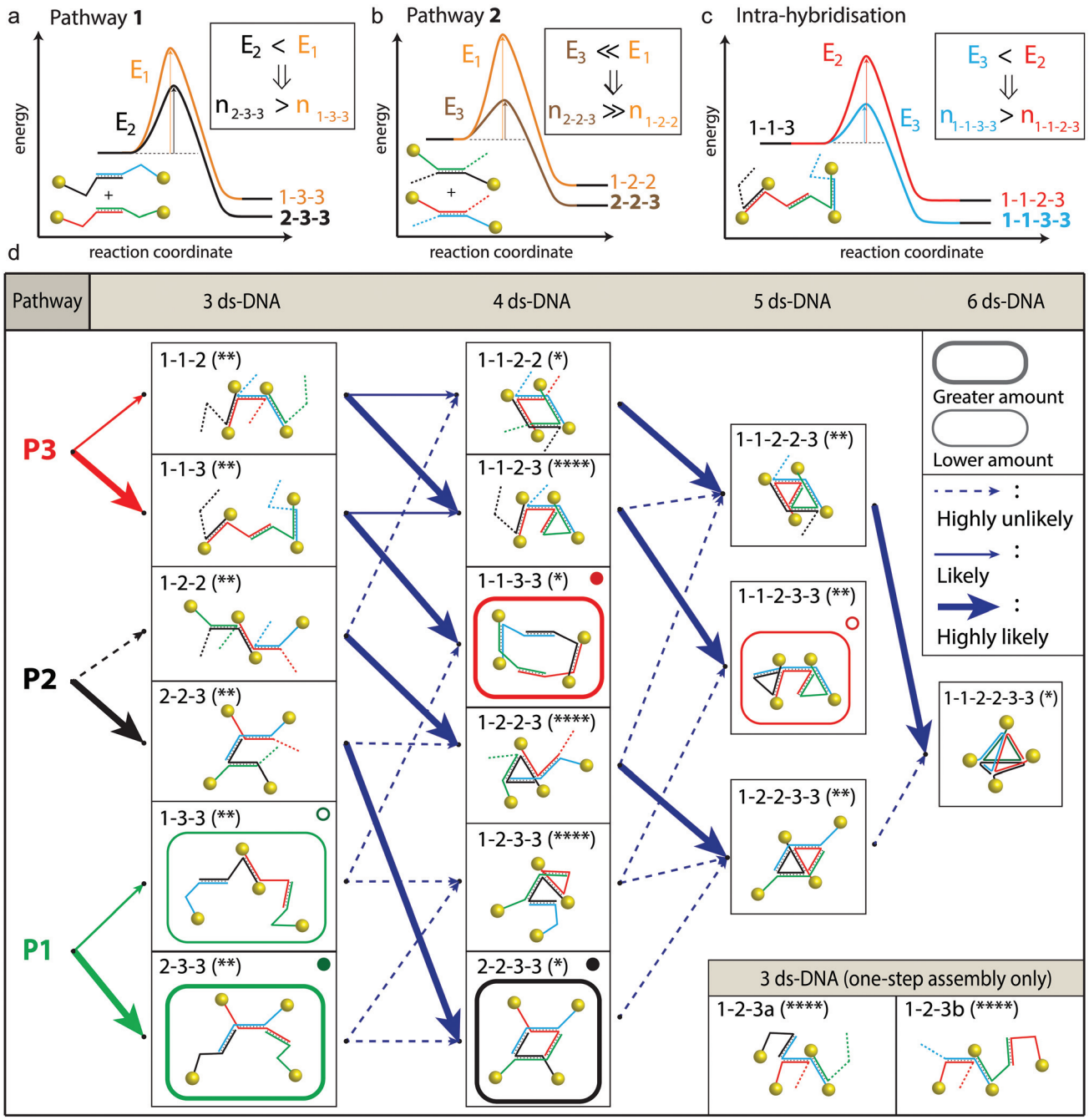

Fig. 2 Hybridisation pathway tree of the symmetrical assembly. (a–c) Energy profile diagrams of (a–b) DNA hybridisation yielding 3 ds-DNA tetramers from dimers for pathways (a) P1, (b) P2 and (c) intra-tetramer hybridisation of isomer 1-1-3. (d) Schematic representation of the 18 possible structural isomers. Single-stranded DNA sub-sequences are represented by a dotted line when one end is free. In the naming system, the subsequence closer to the thiol end of the DNA is numbered 1 and digits (1, 2 or 3) are arranged in an increasing order. The number of asterisks in brackets indicates the total number of tetramer combinations that produce an isomer as detailed in Table 1. In the hybridisation pathway tree, the two red, black and green arrows point to isomers firstly synthesised by pathways P1 to P3 respectively. Blue arrows represent intra-structure hybridisation. Thicker and dotted arrows indicate highly likely and highly unlikely events, respectively. Favoured isomers are circled in different colours depending on the pathway used and the circle thickness indicates the expected relative yield for a given pathway. Circle symbols in the top right corner for the five favoured tetramers are used to identify each tetramer in Fig. 3a–c and 4 to 6.

concentration is likely caused by the irreversible breaking of thiol–Au bonds at high temperature.[48] Moreover, the reduced tetramer yield (observed at both 40 and 90 °C) is explained by an increased number of larger aggregates (Fig. 3d and f), demonstrating that higher temperatures favour inter-structure hybridisation. Further changes to temperatures, salt concentration and salt (NaCl and $MgCl_2$) gave similar results (ESI Fig. S7 and Table S1†).

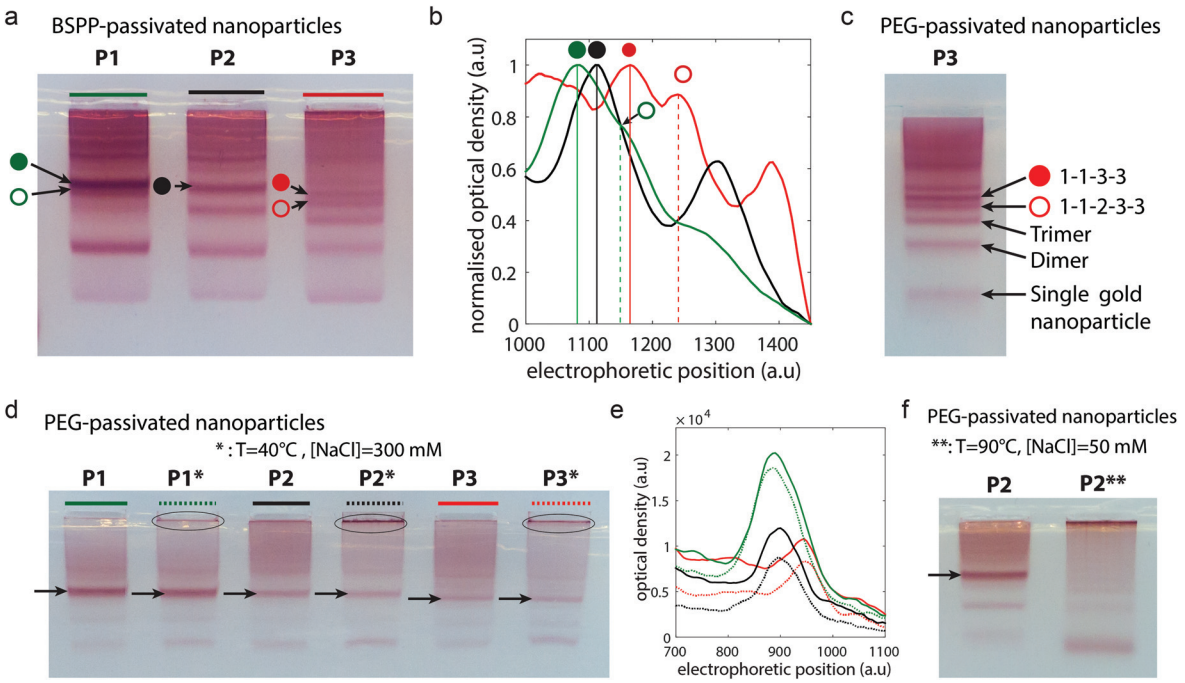

Fig. 3 Structural isomer purification and self-assembly thermodynamics. (a,c) Optimised electrophoretic purification of (a) BSPP- or (c) PEG-passivated gold nanoparticle tetramers synthesised through pathways (a) P1, P2 and (a,c) P3. Arrows indicate the tetramer bands, circles are indicative of specific isomer structures (see Fig. 2d). (b) Normalised cross-sections of panel (a) for pathways P1 (green), P2 (black) and P3 (red). The peak on the right for pathway P1, which appears as a shoulder, was more visible by eye and observed in several experiments (see ESI Fig. S7c†). (d,f) Electrophoretic purification of tetramers synthesised through the pathways P1 (d-green lines), P2 (d-black lines, f) and P3 (d-red lines), prepared at room temperature and [NaCl] = 150 mM (d-solid lines, f-left column), at 40 °C and [NaCl] = 300 mM (d-dotted lines), and at 90 °C and [NaCl] = 50 mM (f-right column). (e) Cross sections of panel (d), centred around the tetramer peak.

3D tetramer arrangement

All isomers possess flexible single-stranded DNA sequences (unhybridised DNA sub-sequences or three-base hinges). The structural flexibility allows the structure the freedom to minimise the overall energy (within the bonding constraints) in 3D *via* the relative positioning of the gold particles. To avoid the drying effects encountered upon preparation of dried samples for conventional TEM, the spatial configuration of four of the five tetrameric isomers in solution was probed *via* cryo-EM along with tilting series (Fig. 4 and ESI Fig. S9–S14†). Statistical analyses of the interparticle distances for all tetramers allows identification of the different structural arrangement of the nanoparticle isomers. For the isomer 1-1-2-3-3, the nanoparticles are linked together with ds-DNA only facilitating identification of the DNA template *via* the interparticle separation and thus precise measurement of ds-DNA lengths (Fig. 5). 207 of 225 tetramers imaged (92%) had at least 3 consecutive interparticle distances compatible with the DNA scaffold. Among those, 153 had also one interparticle distance larger than a single ds-DNA (labelled as C in Fig. 5c). Therefore, A1 and A2 (Fig. 5c) are the pre-assembled dimer axes and B is the location of the hybridisation leading to tetramer formation. By fitting the histograms of the centre-to-centre distances A1 and A2 together (Fig. 5b), and B (Fig. 5c) with a Gaussian distribution convoluted by the diameter distribution and projected in the plane perpendicular to the electron beam,[32,49] we obtained a surface-to-surface distance for A of 8.2 ± 3.5 nm and for B of 7.8 ± 3.8 nm. These distances are slightly shorter than a fully extended 30-base ds-DNA. This is attributed to the high salt concentration used[22,32,49] (100 mM NaCl) and that the DNA scaffold is not necessarily exactly located between the two particles. This statistical analysis matches very well with the DNA template confirming the identity of the isomer. We note this isomer has the lowest hydrodynamic radius and is therefore the most likely to be mistaken with a gold nanoparticle tetrahedron. Full proof that the imaged tetramers are not the 2D projection of a randomly-orientated 3D gold nanoparticle tetrahedron is given in ESI Fig. S18.†

For the isomers 1-1-3-3, 2-2-3-3 and 2-3-3, we measured all six centre-to-centre projected distances between the four gold nanoparticles as the DNA cannot be localised. We estimated average surface-to-surface distances of 10.7 ± 6.0 nm for 1-1-3-3, 12.1 ± 6.8 nm for 2-2-3-3 and 12.9 ± 7.7 nm for 2-3-3 (ESI Fig. S17†). As expected, larger isomers exhibit longer interparticle distances; however, these distances are relatively close given that the electrophoresis bands of these isomers were clearly shifted compared to each other (Fig. 3b). It is likely that the tetramers are more extended in the 0.5% TBE buffer and when travelling in the agarose gel than in salted buffers, due to increased screening of the surface charges.[22,34] These dis-

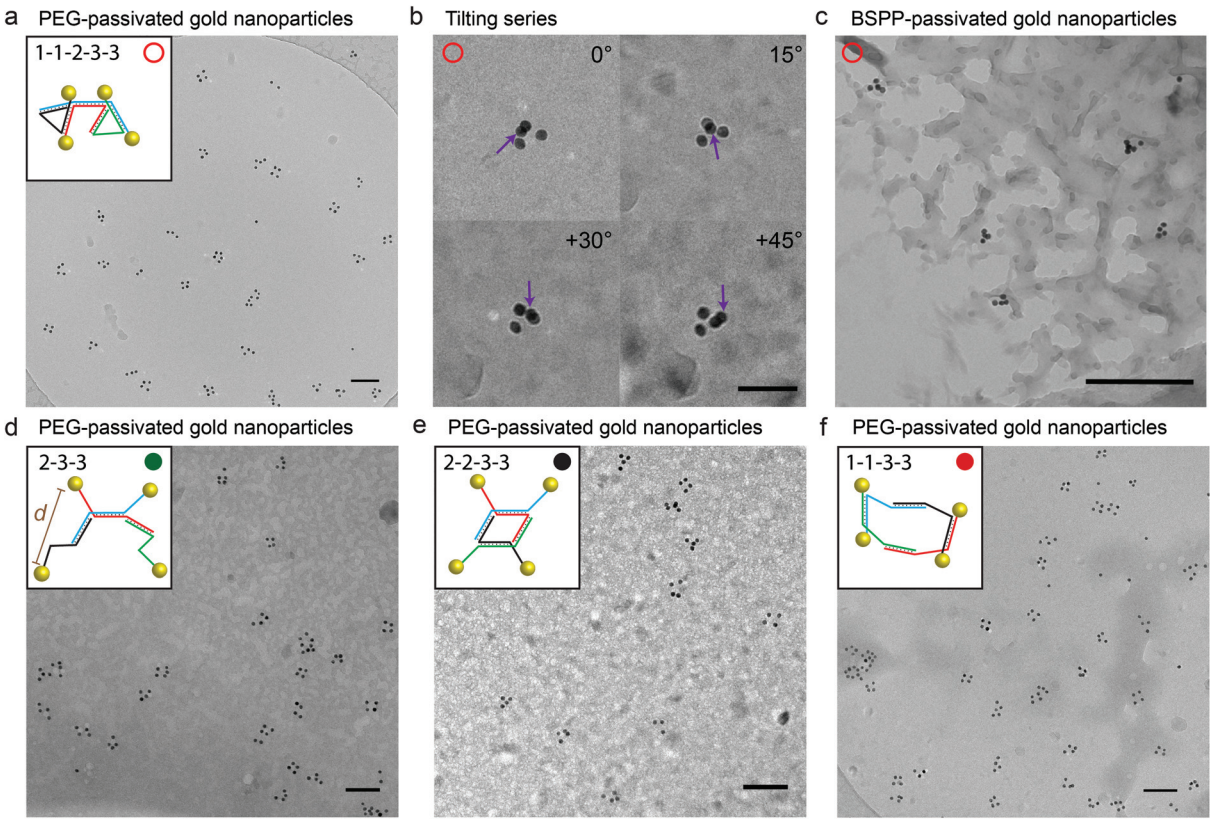

Fig. 4 Structural analysis of tetrameric isomers by widefield cryogenic electron microscopy. Cryo-EM images of (a–b,d–f) PEG- or (c) BSPP-passivated gold nanoparticle isomers (100 mM NaCl concentration); (a–b) 1-1-2-3-3, (d) 2-3-3, (e) 2-2-3-3 and (f) 1-1-3-3. (b) Tilting series of a tetramer exhibiting a 3D configuration: 0° (top left), +15° (top right), +30° (bottom left) and +45° (bottom right). The purple arrow points to the same nanoparticle, the black arrow indicates the tilt direction. Scale bars are 100 nm (a,d–f), 50 nm (b) and 200 nm (c). Insets show the schematised corresponding structures.

tances are also relatively small compared to the size of the fully extended DNA template. For example, in Fig. 4d, the distance noted **d** could reach 85 nm using the classical DNA lengths of respectively 0.34 nm and 0.7 nm per ds- and ss-nucleotide. The DNA average end-to-end distance $\langle r \rangle$ estimated by a worm-like chain (WLC) model,[50] gives a much smaller distance of $\langle r \rangle$ = 17.4 nm. Therefore, the flexibility and random orientation of single-stranded sequences in gold nanoparticle assemblies give leeway to the nanoparticles to position themselves so as to minimise the total energy of the tetramers according to the DLVO theory.[46]

For the small nanoparticles reported here, the ratios between the interparticle distances and particle size are beyond coupling limits and no significant differences in the optical properties of the isomers in solution are observed (see extinction spectra in ESI Fig. S19†). For assemblies of larger particles where coupling is expected to be significant, (*i.e.* diameter >30 nm), each isomer might be expected to possess a characteristic resonant wavelength resulting from the distance-dependant plasmon coupling between the four nanoparticles.

Tetramer assemblies with a tetrahedral geometry are a highly desirable assembly product with potential application in metamaterials[51] due to their unique optical properties.[42,43,52] Nano-assemblies produced by similar tetrahedral DNA templates have been suggested to be 3D tetrahedra using structural analyses[44,53,54] or optical spectroscopy[53,55] measurements, although by-products of partially hybridised structures have been proprosed.[56] Our results show that unique identification of a given isomer is challenging. Moreover, circular dichroism signals may also originate from different tetrameric isomers or from two-nanoparticle interactions in assemblies.[57,58]

Using the above findings, we deposited tetramers into tetrahedra on a substrate by decreasing the interparticle distances within tetramers, using appropriate salt concentrations and surface chemistry, to approximately less than a particle radius, so that one gold nanoparticle deposits on top of the three others (Fig. 6 and ESI Fig. S15†). We used isomers made from BSPP-passivated gold nanoparticles as they have smaller hydrodynamic radii due to the lower repulsion between charged nanoparticles at the same ionic strength (Fig. 4c).

The tetrahedron yields for the different isomers varied from 7 to 28% of all deposited tetramers with the highest yield obtained when depositing the smallest isomer 1-1-2-3-3

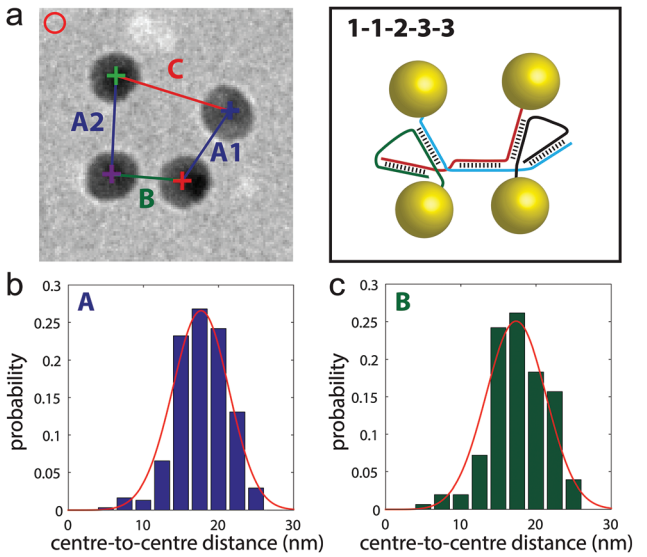

Fig. 5 Statistical analysis of Cryo-EM images. (a) Cryogenic TEM close-up image and corresponding scheme of an isomer 1-1-2-3-3 whose DNA scaffold can be unambiguously identified. A1 and A2 correspond to the center-to-center distances of the pre-assembled dimers, B to the ds-DNA forming the tetramer and C to a distance larger than a 30-base ds-DNA. (b–c) Histograms of centre-to-centre distances (b) A – A1 and A2 together – and (c) B. The red lines correspond to a Gaussian fit taking into account the spatial orientation of the particles with respect to the electron beam.

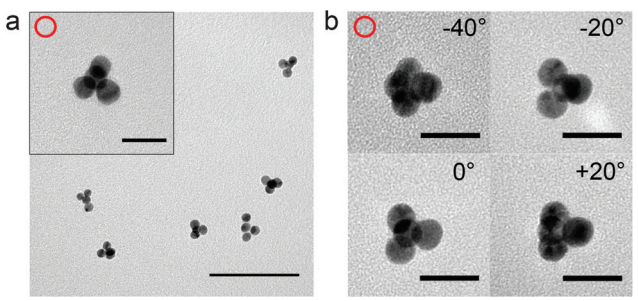

Fig. 6 Tetramers deposited with a tetrahedral geometry. (a) Conventional TEM image of the BSPP-passivated gold nanoparticle isomer 1-1-2-3-3 (200 mM NaCl concentration during deposition). Scale bar is 100 nm. Inset shows a close-up image of a deposited tetrahedron. Scale bar is 20 nm. (b) Tilting series of a deposited tetrahedron: –40° (top left), –20° (top right), 0° (bottom left) and +20° (bottom right). Scale bars are 20 nm.

(Table 2), equivalent to a total yield of 17% among all deposited structures. This is more than an order of magnitude than previously reported.[42,43] Obtaining similar results with a PEG passivation is more difficult because of the steric repulsions between PEG ligands close to contact.[22,34] This demonstrates the active control of the spatial arrangement of the gold nanoparticles using variable surface chemistry and ionic strength.

A potential specific assembly scheme to further optimise the yield of 3D tetrahedral in solution is elucidated by the pathway tree shown in Fig. 2d. The potential pathway exploits the isomer 1-1-2-2, which will intra-hybridise into a tetrahedron. The latter could be produced by pre-hybridising the last 30 bases of the four DNA strands with a 45-base long ss-DNA (blockers), leaving a 15-base long toehold. Following pathway **P3** will produce 1-1-2-2 by preventing the formation of the ds-strand *e* and *f*, and the possibility of removing the blockers.

Conclusions

In summary, we have demonstrated the reproducible synthesis of various kinetically-controlled three-dimensional gold nanoparticle tetramers by sampling the potential energy landscape of nanoparticle-functionalised DNA scaffolds. This approach exploits the numerous possible combinations of self-assembling DNA strands possessing multiple complementary subsequences. We have shown how the steric hindrance introduced by the gold nanoparticles, attached to single DNA strands, drastically modifies the energy landscape of the stepwise DNA hybridisation, favouring the production of specific structural isomers. Unveiling the full hybridisation pathway tree of the self-assembly allowed their identification. Assembling the monoconjugated gold nanoparticle in a different order enables exploring different pathways and produces different structures.

Cryo-EM experiments show that the spatial positioning of nanoparticles within tetramers is facilitated by DNA single-strands and mostly determined by a combination of ionic strength and surface chemistry. Shortening the gold nanoparticle interparticle distances allows the optimisation of conditions to deposit tetramers into tetrahedra on a substrate.

Table 2 Tetrahedron (among tetramers or among all deposited structures) and tetramer yields calculated from TEM images

		Conventional TEM (BSPP passivation) – tetrahedron yield		Cryogenic TEM (PEG passivation)
Pathway	Structure	Among tetramers	Among all deposited structures	Tetramer yield
P1	2-3-3	7% (15/206)	4% (15/364)	61% (189/308)
P2	2-2-3-3	12% (36/298)	6% (36/630)	67% (212/315)
P3	1-1-2-3-3	28% (49/173)	17% (49/297)	45% (307/683)
P3	1-1-3-3	18% (17/92)	13% (17/131)	49% (318/648)

Purified BSPP-passivated gold nanoparticle isomer solutions were deposited for 20 minutes at a NaCl concentration of 100 mM. Tetramer yield among all structures (single particles, dimers, trimers...) of PEG-passivated tetramers calculated from Cryo-EM images.

This nanoparticle self-positioning could reduce the need for large complex templates to make 3D assemblies.

A complete understanding of the underlying parameters controlling DNA-templated nanoparticle self-assemblies paves the way for the use of pathway-controlled approaches[59] to tune and further direct nanoparticle assemblies. It will enable the full translation of the latest advances of DNA nanotechnology[60] such as strand-displacement reactions[61,62] into reversible dynamic nanoparticle assemblies.[63]

In particular, pre-designing hybridisation pathways with a larger number of strands could be used to create a polymorphic DNA that would produce different three-dimensional assemblies depending on which reactants are mixed, and in which order. Moreover, the unhybridised sub-sequences in the kinetically controlled structures could be designed as DNA aptamers[64] or stem-loop[32] to develop multi-receptor optical biosensors.

Materials and methods

General

Thiolated and methyl terminated ethylene glycol hexamer (PEG) was purchased from Polypure (Norway). Solvants and other chemicals were obtained from Sigma-Aldrich. PAGE-purified trithiolated DNA sequences were purchased from Fidelity Systems, Inc. (USA). Salt-free purified monothiolated DNA sequences were obtained from Geneworks (Australia). The DNA sequences are described in ESI.† All chemicals were used as received without further purification. Ultrapure water (18.2 M) was used for all the procedures.

Gold nanoparticle synthesis

The 10 nm gold nanoparticle synthesis was adapted from a protocol detailed in Piella *et al.* (2016).[65] In brief, a 50 mL solution of 2.2 mM trisodium citrate dihydrate containing 33.3 μL of tannic acid (2.5 mM) and 333.3 μL of potassium carbonate (150 mM) was heated at 70 °C in a three-necked round-bottom flask, under vigorous stirring. Then, 333.3 μL of tetrachloroauric acid ($HAuCl_4$, 25 mM) were injected. Growing step: after 15 minutes, 18.5 mL of solution were extracted and replaced by 18.5 mL of 2.2 mM trisodium citrate dihydrate. Once the temperature reached 70 °C again, we added 166.6 μL of $HAuCl_4$ (25 mM) followed by a second identical injection 15 minutes later. This growing step was repeated two or three times. Histograms of the gold nanoparticle diameters are presented in ESI Fig. S16.†

Preparation of gold nanoparticle tetramers

After 24 hours, the as-synthesised nanoparticles were coated with bis(*p*-sulfonatophenyl)phenylphosphine (BSPP)[32,66] and re-concentrated to around 0.3 pmol μL^{-1}. To prepare monoconjugated particles (1 to 8 in Fig. 1a), 90 μL of gold nanoparticle solution were mixed with an excess of monothiolated or trithiolated DNA strands to make a 105 μL solution with 6 mM BSPP and 70 mM NaCl final concentrations. The DNA excess was approximately a 1.5 to 3-fold depending on the DNA strands and was adjusted accordingly for each. All solutions were left to incubate overnight at room temperature. PEG passivation of the nanoparticle surface was achieved by incubation of the particles for 30 minutes in a 100 000 molar excess of PEG prior to electrophoretic purification. In all following electrophoreses, Ficoll 400 (20% solution) is added in a 1 to 5 volume as a loading buffer. Agarose gels were run at 8 V cm^{-1} for about 35–45 minutes with 0.5× Tris-Borate-EDTA as the running buffer (typical 3% agarose gel for this step are shown in ESI Fig. S3†). The extraction procedure was carried out following published protocols[32] and samples were re-concentrated by centrifugation.

Two-step assembly. To form dimers, stoichiometric amounts of BSPP-passivated (resp. PEG-passivated) monoconjugated nanoparticles were mixed overnight at 80 mM (resp. 150 mM) NaCl in a final volume of 15–20 μL. The samples are then electrophoretically purified in 2.5% agarose gels (Fig. 1c and ESI Fig. S3a and b†). Complementary dimers were mixed together overnight in a final volume of 15–20 μL. The standard conditions were 80 mM (resp. 150 mM) NaCl concentration and room temperature.

Single-step assembly. Stoichiometric amounts of monoconjugated 1 to 4 (resp. 5 to 8) were mixed then re-centrifuged down to 15–20 μL and NaCl was added afterwards to obtain a 150 mM concentration for PEG-passivated particles. Samples were incubated overnight at room temperature.

All the samples prepared from the single-step and the two-step assembly are then electrophoretically purified in 2.25% (2.6% in Fig. 3a and c) agarose gels. After extraction and re-concentration, suspensions of tetramers were kept at 50 mM NaCl concentration for stability purposes. As mentioned in the main text, the synthesis of different tetramers was performed at different temperatures and salt concentrations and using different salts (NaCl and $MgCl_2$), as summarised in ESI Table S1.† When a thermal treatment was used, samples were placed at the indicated temperature which slowly decreased overnight.

Electron microscopy

TEM. 20 μL of purified structures were deposited for 10–20 minutes on a holey carbon TEM grid. Following this, excess solution was removed. The grid was washed by sitting for 15 minutes in absolute ethanol. TEM was carried out using a FEI Tecnai G2 T20 TWIN TEM (FEI) using an accelerating voltage of 200 kV. Images were taken with a Gatan SC200D Orius CCD camera (2k × 2k).

Cryo-EM. Samples were prepared using a Vitrobot Mark IV. Gold nanoparticles tetramer suspensions were deposited on holey carbon films (QUANTIFOIL R 2/2 or R 1.2/1.3) that were previously cleaned (PELCO easiGlow). After being blotted with filter paper (the parameters force −10 for 1 second on the instrument gave the best results), the grids are rapidly plunged into liquid ethane and are mounted and inserted in the microscope using a Gatan 626, 70° tilt cryo-transfer holder. Observations were carried out at a temperature of −180 °C in a

Tecnai G2 Spirit TWIN, 120 kV. Images were recorded using a low electron dose on a 4k Eagle CCD. Additional TEM and cryo-EM images are shown in ESI.†

Conflicts of interest

There are no conflicts to declare.

Acknowledgements

This work was supported by the Australian Research Council (ARC) Grants CE170100026 and DP140103011. The authors acknowledge use of facilities within the Monash Centre for Electron Microscopy and within the Monash Ramaciotti Cryo EM platform.

References

1 N. C. Seeman, *J. Theor. Biol.*, 1982, **99**, 237–247.
2 W. M. Shih, J. D. Quispe and G. F. Joyce, *Nature*, 2004, **427**, 618–621.
3 R. P. Goodman, I. A. T. Schaap, C. F. Tardin, C. M. Erben, R. M. Berry, C. F. Schmidt and A. J. Turberfield, *Science*, 2005, **310**, 1661–1665.
4 P. W. K. Rothemund, *Nature*, 2006, **440**, 297–302.
5 Y. He, T. Ye, M. Su, C. Zhang, A. E. Ribbe, W. Jiang and C. Mao, *Nature*, 2008, **452**, 198–201.
6 E. Benson, A. Mohammed, J. Gardell, S. Masich, E. Czeizler, P. Orponen and B. Högberg, *Nature*, 2015, **523**, 441–444.
7 J. Song, J.-M. Arbona, Z. Zhang, L. Liu, E. Xie, J. Elezgaray, J.-P. Aime, K. V. Gothelf, F. Besenbacher and M. Dong, *J. Am. Chem. Soc.*, 2012, **134**, 9844–9847.
8 J.-M. Arbona, J.-P. Aimé and J. Elezgaray, *J. Chem. Phys.*, 2013, **138**, 015105.
9 K. E. Dunn, F. Dannenberg, T. E. Ouldridge, M. Kwiatkowska, A. J. Turberfield and J. Bath, *Nature*, 2015, **525**, 82–86.
10 L. Zhou, A. E. Marras, H.-J. Su and C. E. Castro, *Nano Lett.*, 2015, **15**, 1815–1821.
11 J. M. Arbona, J.-P. Aimé and J. Elezgaray, *J. Chem. Phys.*, 2012, **136**, 065102.
12 W. B. Rogers, W. M. Shih and V. N. Manoharan, *Nat. Rev. Mater.*, 2016, **1**, 16008.
13 J. Chao, Y. Lin, H. Liu, L. Wang and C. Fan, *Mater. Today*, 2015, **18**, 326–335.
14 A. P. Alivisatos, K. P. Johnsson, X. Peng, T. E. Wilson, C. J. Loweth, M. P. Bruchez and P. G. Schultz, *Nature*, 1996, **382**, 609–611.
15 C. A. Mirkin, R. L. Letsinger, R. C. Mucic and J. J. Storhoff, *Nature*, 1996, **382**, 607–609.
16 R. Elghanian, J. J. Storhoff, R. C. Mucic, R. L. Letsinger and C. A. Mirkin, *Science*, 1997, **277**, 1078–1081.
17 J. I. L. Chen, Y. Chen and D. S. Ginger, *J. Am. Chem. Soc.*, 2010, **132**, 9600–9601.
18 K. Keunsuk, O. Jeong-Wook, L. Y. Kwang, S. Jiwoong and N. Jwa-Min, *Angew. Chem., Int. Ed.*, 2017, **56**, 9877–9880.
19 T. Chen, Y. Hong and B. M. Reinhard, *Nano Lett.*, 2015, **15**, 5349–5357.
20 S. Bidault, A. Devilez, V. Maillard, L. Lermusiaux, J.-M. Guigner, N. Bonod and J. Wenger, *ACS Nano*, 2016, **10**, 4806–4815.
21 C. Sönnichsen, B. M. Reinhard, J. Liphardt and A. P. Alivisatos, *Nat. Biotechnol.*, 2005, **23**, 741–745.
22 L. Lermusiaux, V. Maillard and S. Bidault, *ACS Nano*, 2015, **9**, 978–990.
23 X. Shen, A. Asenjo-Garcia, Q. Liu, Q. Jiang, F. J. García de Abajo, N. Liu and B. Ding, *Nano Lett.*, 2013, **13**, 2128–2133.
24 R. Schreiber, N. Luong, Z. Fan, A. Kuzyk, P. C. Nickels, T. Zhang, D. M. Smith, B. Yurke, W. Kuang, A. O. Govorov and T. Liedl, *Nat. Commun.*, 2013, **4**, 2948.
25 Y. Tian, T. Wang, W. Liu, H. L. Xin, H. Li, Y. Ke, W. M. Shih and O. Gang, *Nat. Nanotechnol.*, 2015, **10**, 637–644.
26 M. J. Urban, P. K. Dutta, P. Wang, X. Duan, X. Shen, B. Ding, Y. Ke and N. Liu, *J. Am. Chem. Soc.*, 2016, **138**, 5495–5498.
27 M. Zhao, X. Wang, S. Ren, Y. Xing, J. Wang, N. Teng, D. Zhao, W. Liu, D. Zhu, S. Su, J. Shi, S. Song, L. Wang, J. Chao and L. Wang, *ACS Appl. Mater. Interfaces*, 2017, **9**, 21942–21948.
28 I. Kaminska, J. Bohlen, S. Mackowski, P. Tinnefeld and G. P. Acuna, *ACS Nano*, 2018, **12**, 1650–1655.
29 K. Jin-Woo and D. Russell, *Part. Part. Syst. Charact.*, 2013, **30**, 117–132.
30 T. G. W. Edwardson, K. L. Lau, D. Bousmail, C. J. Serpell and H. F. Sleiman, *Nat. Chem.*, 2016, **8**, 162–170.
31 Y. Zhang, J. Chao, H. Liu, F. Wang, S. Su, B. Liu, L. Zhang, J. Shi, L. Wang, W. Huang, L. Wang and C. Fan, *Angew. Chem., Int. Ed.*, 2016, **55**, 8036–8040.
32 L. Lermusiaux, A. Sereda, B. Portier, E. Larquet and S. Bidault, *ACS Nano*, 2012, **6**, 10992–10998.
33 L. Lermusiaux and S. Bidault, *Langmuir*, 2018, DOI: 10.1021/acs.langmuir.8b00133.
34 L. Lermusiaux and S. Bidault, *Small*, 2015, **11**, 5696–5704.
35 C. Hartl, K. Frank, H. Amenitsch, S. Fischer, T. Liedl and B. Nickel, *Nano Lett.*, 2018, **18**, 2609–2615.
36 Y. Wang, Y. Wang, D. R. Breed, V. N. Manoharan, L. Feng, A. D. Hollingsworth, M. Weck and D. J. Pine, *Nature*, 2012, **491**, 51–55.
37 L. S. Slaughter, B. A. Willingham, W.-S. Chang, M. H. Chester, N. Ogden and S. Link, *Nano Lett.*, 2012, **12**, 3967–3972.
38 Y. Li, Z. Liu, G. Yu, W. Jiang and C. Mao, *J. Am. Chem. Soc.*, 2015, **137**, 4320–4323.
39 J. Sharma, R. Chhabra, A. Cheng, J. Brownell, Y. Liu and H. Yan, *Science*, 2009, **323**, 112–116.
40 R. P. Goodman, R. M. Berry and A. J. Turberfield, *Chem. Commun.*, 2004, 1372–1373.

41 J. Li, H. Pei, B. Zhu, L. Liang, M. Wei, Y. He, N. Chen, D. Li, Q. Huang and C. Fan, *ACS Nano*, 2011, **5**, 8783–8789.
42 S. J. Barrow, X. Wei, J. S. Baldauf, A. M. Funston and P. Mulvaney, *Nat. Commun.*, 2012, **3**, 1275.
43 S. J. Barrow, A. M. Funston, X. Wei and P. Mulvaney, *Nano Today*, 2013, **8**, 138–167.
44 A. J. Mastroianni, S. A. Claridge and A. P. Alivisatos, *J. Am. Chem. Soc.*, 2009, **131**, 8455–8459.
45 C. Chen, W. Wang, Z. Wang, F. Wei and X. S. Zhao, *Nucleic Acids Res.*, 2007, **35**, 2875–2884.
46 J. N. Israelachvili, *Intermolecular and Surface Forces*, Academic Press: Waltham, MA, 2011.
47 J. S. Bois, S. Venkataraman, H. M. T. Choi, A. J. Spakowitz, Z.-G. Wang and N. A. Pierce, *Nucleic Acids Res.*, 2005, **33**, 4090–4095.
48 M. Borzenkov, G. Chirico, L. D'Alfonso, L. Sironi, M. Collini, E. Cabrini, G. Dacarro, C. Milanese, P. Pallavicini, A. Taglietti, C. Bernhard and F. Denat, *Langmuir*, 2015, **31**, 8081–8091.
49 M. P. Busson, B. Rolly, B. Stout, N. Bonod, E. Larquet, A. Polman and S. Bidault, *Nano Lett.*, 2011, **11**, 5060–5065.
50 C. Rivetti, C. Walker and C. Bustamante, *J. Mol. Biol.*, 1998, **280**, 41–59.
51 Y. A. Urzhumov, G. Shvets, J. Fan, F. Capasso, D. Brandl and P. Nordlander, *Opt. Express*, 2007, **15**, 14129–14145.
52 Z. Fan and A. O. Govorov, *Nano Lett.*, 2010, **10**, 2580–2587.
53 S. Li, L. Xu, W. Ma, X. Wu, M. Sun, H. Kuang, L. Wang, N. A. Kotov and C. Xu, *J. Am. Chem. Soc.*, 2016, **138**, 306–312.
54 Q. Chen, J. M. Smith, H. I. Rasool, A. Zettl and A. P. Alivisatos, *Faraday Discuss.*, 2014, **175**, 203–214.
55 W. Yan, L. Xu, C. Xu, W. Ma, H. Kuang, L. Wang and N. A. Kotov, *J. Am. Chem. Soc.*, 2012, **134**, 15114–15121.
56 A. Stern, D. Rotem, I. Popov and D. Porath, *J. Phys.: Condens. Matter*, 2012, **24**, 164203.
57 W. Yan, W. Ma, H. Kuang, L. Liu, L. Wang, L. Xu and C. Xu, *J. Phys. Chem. C*, 2013, **117**, 17757–17765.
58 P. Fu, M. Sun, L. Xu, X. Wu, L. Liu, H. Kuang, S. Song and C. Xu, *Nanoscale*, 2016, **8**, 15008–15015.
59 P. Yin, H. M. T. Choi, C. R. Calvert and N. A. Pierce, *Nature*, 2008, **451**, 318–322.
60 N. C. Seeman and H. F. Sleiman, *Nat. Rev. Mater.*, 2018, **3**, 17068.
61 D. Y. Zhang and G. Seelig, *Nat. Chem.*, 2011, **3**, 103–113.
62 J. P. Sadowski, C. R. Calvert, D. Y. Zhang, N. A. Pierce and P. Yin, *ACS Nano*, 2014, **8**, 3251–3259.
63 Z. Qian and D. S. Ginger, *J. Am. Chem. Soc.*, 2017, **139**, 5266–5276.
64 P. F. Xu, A. M. Hung, H. Noh and J. N. Cha, *Small*, 2013, **9**, 228–232.
65 J. Piella, N. G. Bastús and V. Puntes, *Chem. Mater.*, 2016, **28**, 1066–1075.
66 D. Zanchet, C. M. Micheel, W. J. Parak, D. Gerion and A. P. Alivisatos, *Nano Lett.*, 2001, **1**, 32–35.